Marine Pollution Bulletin 88 (2014) 292–301

Contents lists available at ScienceDirect

Marine Pollution Bulletin

journal homepage: www.elsevier.com/locate/marpolbul

Environmental policy constraints for acidic exhaust gas scrubber discharges from ships

H. Ülpre *, I. Eames

University College London, Torrington Place, London WC1E 7JE, United Kingdom

ARTICLE INFO

Article history:
Available online 3 October 2014

Keywords:
Turbulent jet
Acid–alkali chemistry
Scrubber
Seawater

ABSTRACT

Increasingly stringent environmental legislation on sulphur oxide emissions from the combustion of fossil fuels onboard ships (International Maritime Organization (IMO) Regulation 14) can be met by either refining the fuel to reduce sulphur content or by scrubbing the exhaust gases. Commonly used open loop marine scrubbers discharge warm acidic exhaust gas wash water into the sea, depressing its pH. The focus on this paper is on the physics and chemistry behind the disposal of acidic discharges in seawater.

The IMO Marine Environment Protection Committee (MEPC 59/24/Add.1 Annex 9) requires the wash water to reach a pH greater than 6.5 at a distance of 4 m from the point of discharge. We examine the engineering constraints, specifically size and number of ports, to identify the challenges of meeting regulatory compliance.

1. Introduction

The main products in the combustion of fossil fuels in air are carbon oxides (CO_x) and water (H_2O). The most common by-products are sulphur oxides (SO_x), nitrogen oxides (NO_x) and carbon based matter (soot, smoke). The by-products exist in small quantities but have a disproportionate effect on the environment. SO_x is generated in combustion due to sulphur compounds that have not been removed from the fossil fuels. NO_x is the result of combustion at high temperatures and the carbon based matter (*e.g.* CO_x, soot) is formed due to incomplete combustion. All of these by-products are polluting and their release, therefore, has to be mitigated. The absorption of CO_2 by seawater is the main reason for anthropogenic ocean acidification (Raven et al., 2005). Shipping accounts for 2.7% of the global total CO_2 emissions and as of January 1st 2013 (IMO, 2009). As a result the IMO has implemented mandatory measures to increase the energy efficiency of new ships (MEPC 62/24/Add.1 Annex 19). NO_x emissions fall under IMO Regulation 13 and a number of methods can be used to meet the emission limits (Blatcher and Eames, 2013). IMO Regulation 14 dictates the emission limits for SO_x and carbon particles from ships. Naturally occurring low sulphur fuel is scarce and refining to reduce sulphur content is expensive. An alternative is to use cheaper high sulphur content fuel in combination with an exhaust gas scrubbers to mitigate SO_x emissions.

Commonly used exhaust gas scrubbers on ships are open loop meaning that seawater is taken onboard, used to clean the exhaust gases and then discharged back into the ambient. The principle of the scrubber (see Fig. 1) is to spray the flue gas with seawater capturing the carbon particles as well as the SO_x gas that forms sulphuric acid (H_2SO_4) on contact with water. Before the wash water's discharge into the ambient, it is filtered from sludge created by carbon particles and other particulate fuel impurities. Depending on onboard treatment and discharge pipe configuration it is likely that the wash water will be in the form of a warm acidic jet. The immediate effects of the acidic discharge are mitigated due to rapid pH recovery back to ambient levels in the vicinity of the discharge nozzle. The long term effects are out of the scope of this paper.

Emissions Control Areas (ECA), shown in Fig. 2a, cover the Pacific and Atlantic coasts of the United States and Canada, the Gulf of Mexico, Hawaiian Islands and the North and Baltic seas. The ECA are defined in MEPC 60/22 Annex 11 for the Americas and the limits of the North Sea are defined by the International Hydrographic Organization. In these regions the SO_x emissions limits are very severe (a maximum of 1% of fuel weight can be sulphur as of 1st of July 2010) meaning that exhaust gas scrubbers are likely to be used. Outside of the ECA the sulphur content can be up to 3.5% of fuel weight. Modern diesel and gas turbine ships are supported by auxiliary engines that are used for electricity generation and manoeuvring. Depending on the size of the ship a number of scrubbers may be fitted to allow for the independent running of main

* Corresponding author.
E-mail address: h.ulpre@ucl.ac.uk (H. Ülpre).

http://dx.doi.org/10.1016/j.marpolbul.2014.08.027
0025-326X/

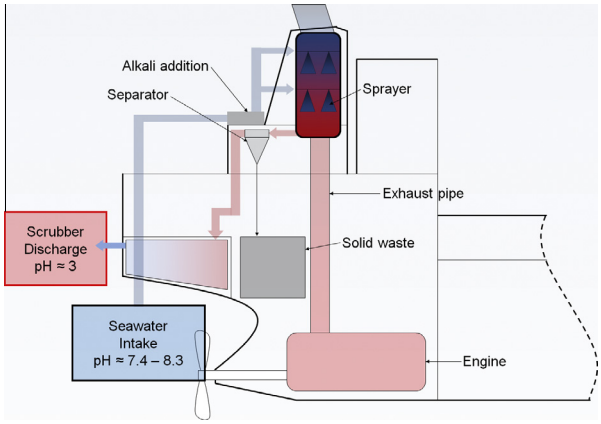

Fig. 1. Schematic of a typical wet open loop exhaust gas scrubber setup.

and auxiliary engines. The acidic scrubber discharges need to comply with the MEPC 59/24/Add.1 Annex 9 regulation:

> The wash water pH should comply with one of the following requirements which should be recorded in the ETM-A or ETM-B as applicable:
>
> (I) The discharge wash water should have a pH of no less than 6.5 measured at the ship's overboard discharge with the exception that during manoeuvring and transit, the maximum difference between inlet and outlet of 2 pH units is allowed measured at the ship's inlet and overboard discharge.
>
> (II) During commissioning of the unit(s) after installation, the discharged wash water plume should be measured externally from the ship (at rest in harbour) and the discharge pH at the ship's overboard pH monitoring point will be recorded when the plume at 4 m from the discharge point equals or is above pH 6.5. The discharged pH to achieve a minimum pH units of 6.5 will become the overboard pH discharge limit recorded in the ETM-A or ETM-B.

The acronyms ETM-A and ETM-B refer to technical manuals from the manufacturer (EGC system – Technical Manual). The seawater pH varies approximately from 7.5 to 8.5 meaning that a discharge of fluid at a pH of 5.5 is permitted in certain conditions (*e.g.* north-eastern regions of the Baltic Sea) in the case of (I). However, in the case of (II) there is no limit to the discharge pH as long as it recovers to a pH of 6.5 within a distance of 4 m from the nozzle.

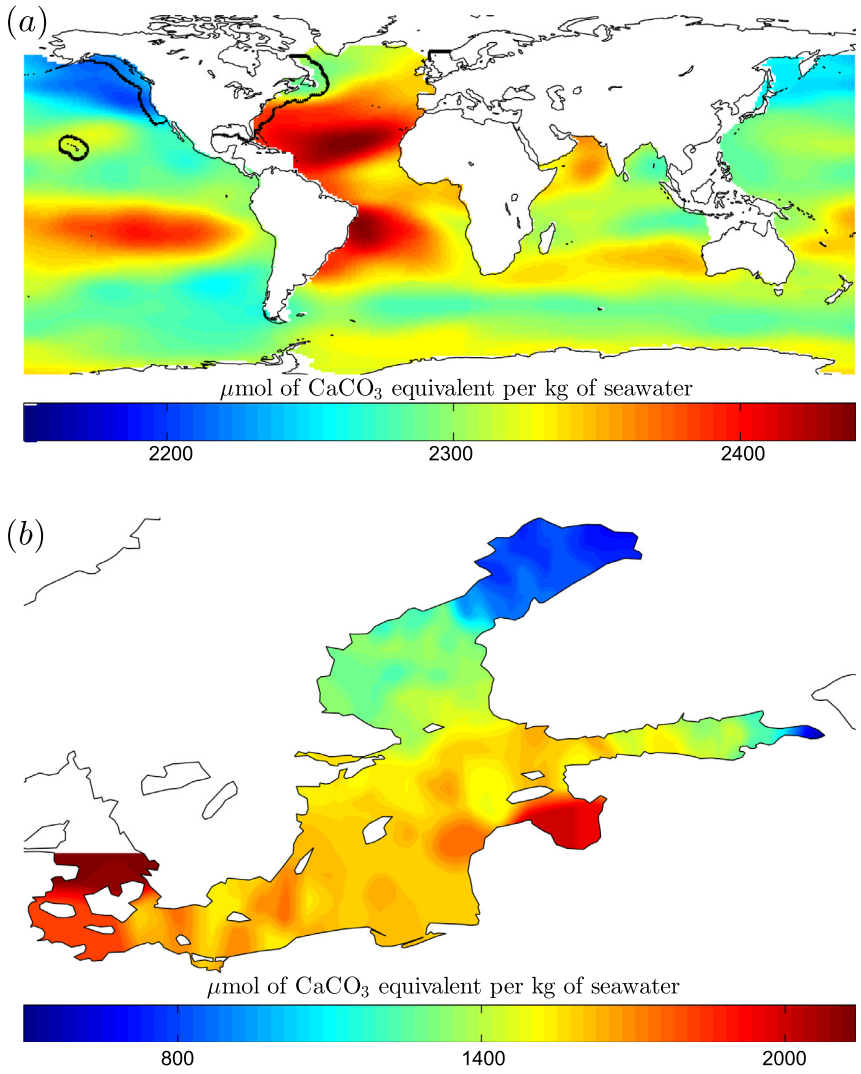

Fig. 2. In (a), the global estimate of the total potential seawater alkalinity (μmol/kg) based on seawater salinity (Key et al., 2004). The Emissions Control Areas (ECA) are highlighted with thick black lines. In (b), the estimate of the average seawater alkalinity (μmol/kg) between 2000 and 2012 in the Baltic Sea (ICES, 2011). The Savitzky–Golay filter was applied to the data in Matlab R2013b.

Regulatory compliance is demonstrated by measuring the pH at a fixed depth and 4 m in front of the discharge port while the ship is held at rest with its engines running and driving the propeller. This means that an ambient flow will be present deviating the discharge in combination with buoyancy originating from the wash water's contact with hot exhaust gases. The focus of this paper is on the pH recovery of scrubber discharges, however, in order to fully comply with the legislation the measurements of PAH (oil content), turbidity and temperature also need to be monitored and controlled. We will be addressing case (II) because it allows for a lower discharge pH and we also analyse the discharge deviation due to temperature and ambient flow up to 4 m from the nozzle.

Wash water pH recovery depends in part on the chemical composition of seawater and on the amount of dilution. Seawater is a weak alkaline buffer solution which contains a large number of dissolved salts (Drever, 1988), some of which affect its pH. Alkaline buffer solutions resist changes to pH by absorbing hydrogen ions (H^+) when small amounts of acid are added. The majority of the seawater buffering capacity comes from carbonate (CO_3^{2-}) and bicarbonate (HCO_3^-) ions. Calcium carbonate ($CaCO_3$) is a sparingly soluble alkaline salt that is very common in seawater, therefore, the seawater alkalinity is frequently estimated in calcium carbonate equivalent moles. Seawater's buffering capacity is also influenced by temperature, depth, salinity and coastal runoffs. For example, glacial ice melting in the summer introduces fresh water into seawater reducing the acid buffering capacity. Typical values of seawater alkalinity around the globe range from 2200 to 2400 μmol/kg (Fig. 2a). In parts of the Baltic Sea, however, alkalinity is far lower at 800 μmol/kg (Fig. 2b). The brackish characteristic of the Baltic Sea is due to the large number of rivers flowing into it and the limited exchange with the North Sea. Additionally, the seawater alkalinity is slightly lower near the free surface because of carbonic acid produced from the absorption of atmospheric carbon dioxide. Marine organisms frequently experience pH fluctuations but prolonged periods of depressed pH can cause considerable harm (Knutzen, 1981), therefore, the scrubber discharge pH recovery must occur very rapidly.

This paper is structured as follows: in Section 2, we describe mathematical fluid flow and chemistry models that describe the behaviour of acidic jets and plumes in an alkaline environment. In Section 3, design solutions are proposed to satisfy the necessary IMO MEPC guidelines for acidic discharges which take into account the discharge acidity, required flow rate, seawater alkalinity, ship power, the size of the discharge port and dilution prior to discharge. Conclusions are presented in Section 4 and the titration procedure that is critical to determining the seawater buffering capacity is described in Appendix A.

2. Physics of dilution

Consider a scrubber generating an acidic effluent from seawater with a volume flux Q_s and acidity C_a^s. Onboard the ship, the wash water may be diluted with an additional Q_w resulting in a total volume flux $Q_0 = Q_s + Q_w$ at the point of discharge. The onboard dilution factor $D_{onboard}$ and the resulting acidity C_a^0 at the point of discharge are

$$D_{onboard} = \frac{Q_w}{Q_s}, \quad C_a^0 = \frac{(C_a^s - C_b^0)Q_s}{Q_s + Q_w}, \tag{1a, b}$$

where C_b^0 is the alkalinity of the ambient seawater. The inclusion of $D_{onboard}$ may be useful to ensure pH recovery in especially low seawater alkalinity regions. At the outlet Q_0 can be increased with a larger number of nozzles N

$$Q_0 = Q_s(1 + D_{onboard}) = \pi b_0^2 u_0 N, \tag{2}$$

where b_0 is the radius of the nozzle and u_0 is the discharge velocity. Between the wash water leaving the ship and reaching a distance of 4 m, the fluid has been diluted by a factor of D_{jet}. The total dilution (D_T) that has occurred from the scrubber to the distance of 4 m from the discharge nozzle is

$$D_T = (1 + D_{jet})(1 + D_{onboard}) - 1. \tag{3}$$

In a time averaged jet D_{jet} indicates the amount of dilution on the jet centre line, a region where dilution will be at it's lowest.

2.1. Constraints on velocity

Two characteristic velocities are of importance in this problem, the flow velocity in the discharge pipes u_p and the discharge jet velocity u_0 at the nozzle. The constraint on the flow within the pipe is that cavitation does not occur, requiring that the pressure P satisfies

$$P\left(= P_a + \rho g h - \frac{\rho u_p^2}{2}\right) > P_v, \tag{4}$$

where P_v is the cavitation pressure of the water, P_a is the atmospheric pressure, ρ is the the density of the water, g is acceleration due to gravity and h is the depth of discharge. Observations on the phenomena of cavitation were first published by Reynolds (1873). The potential to cavitate depends on water depth, water quality and the smoothness of the pipe internal surface. The flow speed can be increased by reducing the friction coefficient of the pipe through *e.g.* acrylic coating. The outlet nozzle radius can be designed to be much smaller than the discharge pipe radius, therefore, u_0 can be much higher than u_p, however, additional material considerations need to be taken into account (Krivchenko, 1994). Entrainment is a mechanism leading to the growth of the jet radius and volume flux with distance from the point of discharge through the capture of ambient fluid (Hunt et al., 2011). At low discharge velocities the jet becomes laminar, the consequence of this is that mixing with ambient fluid is significantly reduced due to the dominance of viscous forces (Batchelor, 2001). Entrainment models for laminar jets are discussed by Morton (1967). In order to obtain optimal dilution through turbulent mixing we introduce a constraint

$$Re\left(= \frac{2 b_0 u_0}{\nu}\right) > Re_c, \tag{5}$$

where Re_c is a critical Reynolds number and ν is the kinematic viscosity of water. Certainly $Re_c = 3000$ is sufficient for the jet to be turbulent (McNaughton and Sinclair, 1966).

2.2. Buoyant jet model

We describe a mathematical model of a buoyant jet discharged horizontally and tangentially into a uniform unstratified stream in order to calculate the jet trajectory and dilution. An unstratified ambient is considered because the draught depth of merchant vessels is at most 20 m and in this range the effects of stratification are not significant. It is assumed that the issuing fluid is perfectly mixed across the width of the jet and that the dilution processes have a far longer timescale than the chemical processes that happen very rapidly (Ülpre et al., 2013). In the 'top-hat' model (Morton et al., 1956), the jet is characterized by a radius b, average centre line velocity u and a density contrast of $\rho - \rho_a$ compared to the ambient ρ_a. These variables are combined to form the volume flux Q, specific momentum flux M and specific buoyancy flux B, which are defined as

$$Q = \pi b^2 u, \quad M = \pi b^2 u^2, \quad B = \pi b^2 u g\left(\frac{\rho_a - \rho}{\rho_a}\right). \tag{6a, b, c}$$

The initial values of Q, M and B at the point of discharge are Q_0, M_0 and B_0. The conservation of mass and momentum are expressed in terms of how Q and M vary with distance s along the jet trajectory. The jet is directed along the y-axis, rises due to buoyancy along the z-axis and is swept by an ambient flow along the x-axis. Two forces act on the buoyant jet in the presence of an ambient flow U_∞, the Lamb force and buoyancy. In conclusion this gives

$$\begin{aligned} &\frac{\mathrm{d}Q}{\mathrm{d}s} = 2\pi u_E b, \quad \frac{\mathrm{d}}{\mathrm{d}s}\left(M\frac{\mathrm{d}x}{\mathrm{d}s}\right) = 2\pi u_E U_\infty b, \\ &\frac{\mathrm{d}}{\mathrm{d}s}\left(M\frac{\mathrm{d}y}{\mathrm{d}s}\right) = 0, \quad \frac{\mathrm{d}}{\mathrm{d}s}\left(M\frac{\mathrm{d}z}{\mathrm{d}s}\right) = \pi b^2 g\left(\frac{\rho_a - \rho}{\rho_a}\right), \end{aligned} \tag{7}$$

where u_E is the entrainment velocity that must be closed by an empirical relationship between the mean jet velocity and the ambient flow (da Silva et al., 2014). We use the closure relationship applied by Woodhouse et al. (2013)

$$u_E = \alpha\left(\left|u\frac{\mathrm{d}z}{\mathrm{d}s}\right| + \left|u\frac{\mathrm{d}x}{\mathrm{d}s} - U_\infty\right| + \left|u\frac{\mathrm{d}y}{\mathrm{d}s}\right|\right), \tag{8}$$

but others have also been proposed *e.g.* Jirka (2004). Since the discharges are likely to be in the form of jets we can assume the empirically determined entrainment coefficient to be $\alpha = 0.08$ (Turner, 1969). The temperature difference between the discharge and the ambient seawater generates buoyancy, in this case the ambient temperature is taken as 10 °C and the temperature difference between the ambient and the discharge is $\Delta T_0 = 5$, 10, 20 and 30 °C. The values of ΔT_0 result in the density contrast at the nozzle $((\rho_a - \rho_0)/\rho_a)$ of 0.0006, 0.0015, 0.0040 and 0.0075 kg/m^3 for Standard Mean Ocean Water (SMOW) (Tanaka et al., 2001). The system of equations in (7) is solved using the Euler method in Matlab R2013b for $b_0 = 0.05$ m, the results are plotted in Fig. 3 and discussed in the following section.

2.3. Reduced model for a horizontal jet

For large initial jet velocities (*i.e.* $u_0 \gg \sqrt{g b_0(\rho_a - \rho_0)/\rho_a}, U_\infty$) the influence of buoyancy and ambient flow is negligible in the

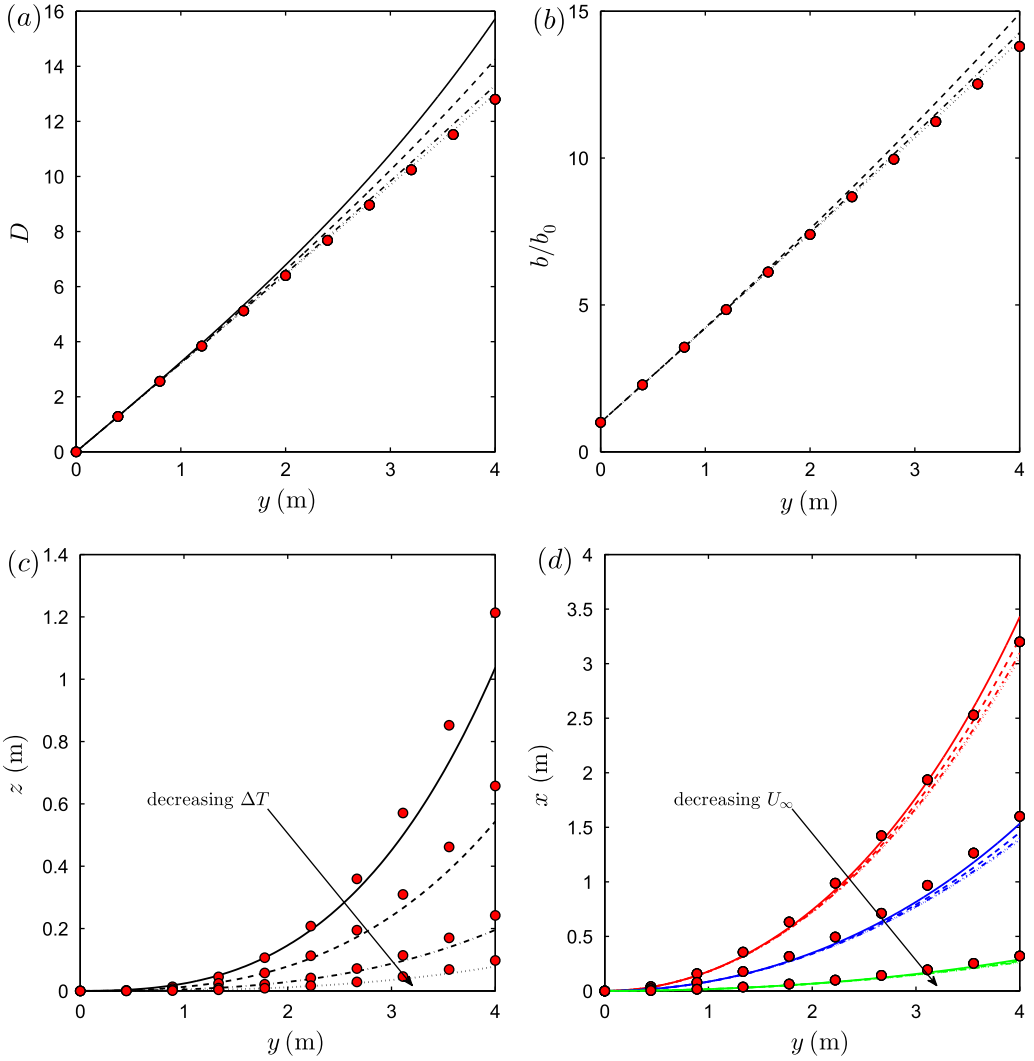

Fig. 3. A comparison is shown between the model presented in Section 2.2 and the reduced expressions in Section 2.3. The influence of buoyancy with $b_0 = 0.05$ m and $u_0 = 2$ m/s is investigated for $\Delta T_0 = 5$ °C (dotted line), 10 °C (dash–dot line), 20 °C (dashed line), 30 °C (solid line) on all of the subplots. The red circles in (a) and (b) correspond to (9b) and (9a) respectively. In (c), the influence of buoyancy on the deflection of the jet along the z-axis is compared with (14) plotted as red circles. In (d), the influence of buoyancy and U_∞ on the deflection of the jet along the x-axis is compared with (16) plotted as red circles. The red, blue and green sets of lines correspond to $U_\infty/u_0 = 0.1$, 0.05 and 0.01. (For interpretation of the references to colour in this figure legend, the reader is referred to the web version of this article.)

near field. The benefit of a high discharge velocity is that it also results in a more coherent jet within 4 m from the nozzle. In this limit, from (7), the following linear relationships can be established

$$\frac{b}{b_0} = 1 + D_{jet}, \quad D_{jet} = \frac{2\alpha y}{b_0}. \tag{9a, b}$$

Jet dilution and volume flux increase (Morton et al., 1956) along the centre line are related to each other through the following relationship

$$\frac{Q}{Q_0} = 1 + D_{jet}. \tag{10}$$

The comparison with the full model in Section 2.2 and the estimates in (9a,b) are plotted in Fig. 3a and b. The jet forms a conical shape with an angle $\tan^{-1}(4\alpha) = 17.74^\circ$. Over a distance of $y = 4$ m, the jet fluid has been diluted by a factor of

$$D_{jet} = \frac{0.64}{b_0}. \tag{11}$$

The decay in u and ΔT of the jet with distance y due to entrainment of ambient fluid (dilution) can be estimated as

$$\frac{u}{u_0} = \frac{1}{1 + \frac{2\alpha y}{b_0}}, \quad \frac{\Delta T}{\Delta T_0} = \frac{1}{1 + D}. \tag{12a, b}$$

By inserting the terms in (9a) and (12a) into (5) it can be shown that the local Reynolds number within a momentum dominated jet cone will stay constant, so if the jet is initially turbulent at the outlet it will be turbulent along its path.

When measuring the location of the jet centre line at 4 m it is important to make a correction due to the effect of U_∞ and ΔT. The influence of ΔT causes the jet to rise above the point of discharge. This rise can be estimated from

$$M_0 \frac{d^2 z}{dy^2} \simeq \pi b^2 g \left(\frac{\rho_a - \rho_0}{\rho_a} \right). \tag{13}$$

Since the buoyancy flux is conserved, we can integrate (13) to obtain

$$z \simeq \frac{g y^2}{u_0^2} \left(\frac{1}{2} + \frac{\alpha y}{3 b_0} \right) \left(\frac{\rho_a - \rho_0}{\rho_a} \right), \tag{14}$$

where the distance z is the amount the jet has risen. Similarly the jet trajectory deflection due to a weak cross flow is estimated from

$$M_0 \frac{d^2 x}{dy^2} \simeq 2\pi u_E U_\infty b_0 \simeq 2\pi \alpha u_0 U_\infty b_0, \tag{15}$$

where entrainment (u_E) is simplified to αu_0. Integrating (15) results in an approximation for the jet deflection downstream

$$x \simeq \frac{\alpha U_\infty y^2}{u_0 b_0}. \tag{16}$$

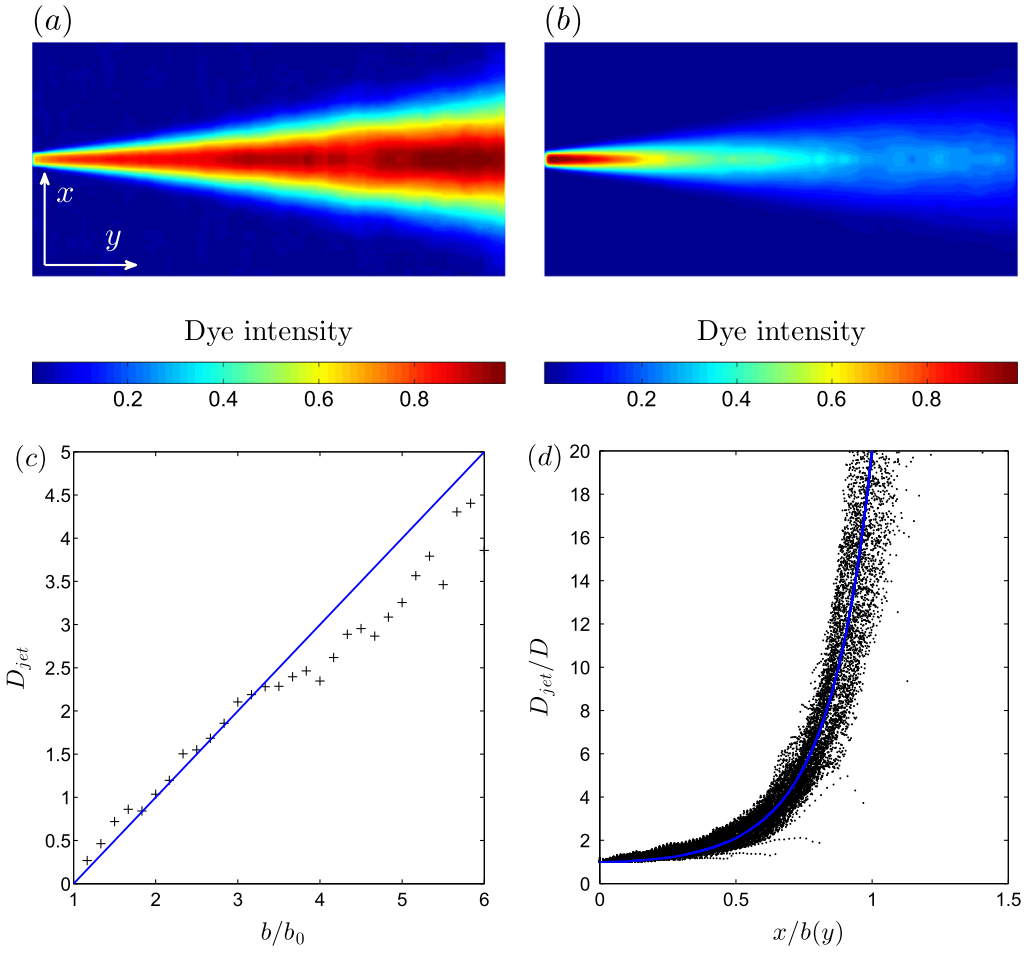

Fig. 4. In (a), a depth integrated and time averaged image of an experimental jet with passive dye. In (b), an inverse Abel transformation (17) is performed and to extract the average dye concentration through the centre line. The dye intensity is given in the range of minimum to maximum *i.e.* 0–1. In (c), the dilution is plotted against distance along the jet trajectory and the solid blue line corresponds to (9a). In (d), the dye dilution is related to the tangential distance from the jet centre line and the solid blue line corresponds to (21). (For interpretation of the references to colour in this figure legend, the reader is referred to the web version of this article.)

A comparison between the full numerical model in Section 2.2 and (14) and (16) is shown in Fig. 3c and d respectively. The agreement is good for $|\Delta T_0| < 20$ °C and $U_\infty/u_0 < 0.01$. The previous discussion gives practical estimates of the centre line dilution.

Additional information is required to understand how average dilution varies across the jet width. To examine this effect we analysed the dilution of a jet containing passive dye as it is gradually diluted. The experiments were performed in a large 650 L tank with the jet issuing from a nozzle with $b_0 = 0.022$ m. A colour camera recorded depth integrated images at 25 frames per second which were then time averaged over a period of 7 s. Fig. 4a shows an image of a jet containing passive dye and provides information about the depth integrated and time averaged dye concentration $C_{DI}(x,y)$. An inverse Abel transformation (Abel, 1826) was performed to reconstruct the axisymmetric form of the dye concentration through the jet using

$$\overline{C}(x,z) = -\frac{1}{\pi}\int_r^\infty \frac{\mathrm{d}\overline{C}_{DI}}{\mathrm{d}m}\frac{\mathrm{d}m}{\sqrt{m^2-r^2}}. \tag{17}$$

Fig. 4b shows the reconstructed concentration profile. It has been known that the time averaged concentration field $\overline{C}$ across the jet is approximately Gaussian (*e.g.* Morton et al. (1956), *etc.*) *i.e.*

$$\overline{C} = \frac{\overline{C}_0}{1+(2\alpha y/b_0)}\exp\left(-\frac{\lambda x^2}{b^2}\right). \tag{18}$$

The dilution at any location in the jet $D(x,y)$ can be estimate by relating the centre line concentration C to the value at the nozzle C_0 and radius b to the value that captures 95% of the jet fluid giving $\lambda = \log(1/0.05) \simeq 3$. This relationship can, therefore, be expressed as

$$D_{jet} = \frac{\overline{C}_0}{\overline{C}} - 1. \tag{19}$$

Fig. 4c shows variation of the centre line jet concentration with jet radius, confirming (9a). The depth integrated concentration is related to the concentration profile

$$D(x,y) = \left(1+\frac{2\alpha y}{b_0}\right)\exp\left(\frac{3x^2}{(b_0+2\alpha y)^2}\right) - 1. \tag{20}$$

Fig. 4d confirms (20) a rapid increase in dilution as we move away from the centre line, the expression for the solid line is

$$\frac{D_{jet}}{D} = \exp\left(-\frac{\lambda x^2}{b^2}\right). \tag{21}$$

2.4. Chemistry of reactions

The chemical properties of seawater are usually characterised in terms of alkalinity and pH. The total seawater alkalinity in a sample is defined as the number of hydrogen ion moles equivalent to the excess of proton acceptors; physically it is the concentration of a strong monoprotic acid C_a^0 (of equal volume to the seawater sample). The chemistry is complicated because many of the alkaline salts are sparingly soluble in water. The pH of a strong alkaline solution is sensitive to the alkaline salt concentration but for a weak alkaline solution, the salt dissociativity K_b must be taken into account. A typical weak alkali, sodium carbonate, has $K_b = 10^{-4.67}$ mol^2/l^2 while the K_b for a strong alkali is greater than unity. The pH of a solution is defined in terms of the molar concentration of pH $= -\log_{10}[\mathrm{H}^+]$. For an acid reacting with an alkali, the hydrogen ion concentration is

$$[\mathrm{H}^+] = \frac{C_a^0 - DC_b^0}{1+D}. \tag{22}$$

A neutral pH is temperature dependant and varies from pH = 7.47 at 0 °C, pH = 7 at 25 °C and pH = 6.92 at 30 °C. The effect of adding an alkali (*e.g.* seawater) to the acidic solution decreases the hydrogen ion concentration (*i.e.* increase the pH). The point of neutralisation is determined by chemistry alone (*i.e.* $D_N = C_a^0/C_b^0$) but the process of reaching the point of neutralisation is determined both by chemistry, the numerator of (22), and dilution, the denominator of (22).

To understand how the pH of acidified seawater varies as it is gradually diluted with seawater, a series of titration experiments were undertaken. These titration curves allow us to interpret the seawater alkalinity in terms of a strong monoprotic alkali and are of singular importance in trying to understand pH recovery from acidic jets. They must be obtained from experiments – the instructions for undertaking these titrations are given in Appendix A. Seawater samples were taken from the River Thames and Brighton Marina. The 100 ml samples of river/seawater were acidified with 4 ml of 1 mol/l nitric acid (HNO_3) resulting in pH = 3.27 for Thames water and pH = 3.45 for Brighton Marina. For low dilution factors, the dependence of pH on dilution is similar for both samples (see Fig. 5a and b) because the molarity of the acid is much stronger

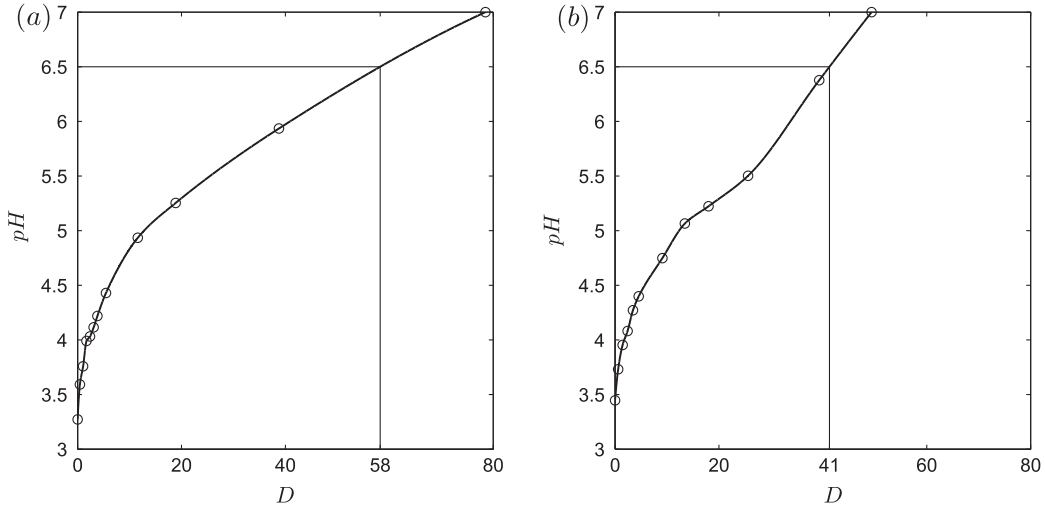

Fig. 5. Empirical titration curves (Ülpre et al., 2013) with a cubic spline fitted to the data, for acidified (a) Thames River and (b) Brighton marina water samples. The samples were acidified with nitric acid resulting in pH = 3.27 for Thames water and pH = 3.45 for Brighton Marina. The number of points indicates the number of dilutions performed for the solution to become slightly alkaline (pH ≈ 7).

than the alkalinity; in this instance the initial pH increase is largely due to dilution with the pH recovering by slightly more than 1 unit when $D = 10$. From these curves we can determine the total dilution required to bring the discharge to a pH = 6.5.

In this example, Brighton seawater has an alkalinity of 770 μmol/l and River Thames water has an alkalinity of 480 μmol/l. The former is typical for the low alkalinity waters in the Baltic seas (see Fig. 2b). These titration experiments were done over a period of 15 min, with less than a minute for each step; much faster than a number of published studies (Behrends et al., 2005). This is to mimic more closely the processes that occur within the jet – the travel time of the acidic jet fluid from the nozzle to a distance of 4 m is typically <10 s.

3. Design implications

We examine the engineering constraints on D_{jet} and chemistry constraints on D_T to achieve the necessary pH recovery. The design of the port discharge hole may be optimised to ensure pH = 6.5 at 4 m, for a single circular discharge port. An example discharge of pH = 3.5 is used, which was obtained from mixing seawater and a monoprotic acid with molarity 0.0385 mol/l. Extension to other values of discharge pH and seawaters is straightforward.

3.1. Without prior dilution or treatment ($D_{onboard} = 0$)

To enable large volumes to be discharged multiple ports may be required and the number can be estimated to be

$$N = \frac{Q_s D_T^2}{4\pi u_0 \alpha^2 x^2}. \tag{23}$$

From (11), the jet nozzle radius that ensures a dilution D_T, is

$$b_0 = \frac{2\alpha x}{D_T}. \tag{24}$$

Fig. 6 shows how the number and size of the discharge ports is selected. We consider the examples of 5, 10 and 15 MW ships (where $Q_s = 45$ t/hr per MW of power) which are in waters with

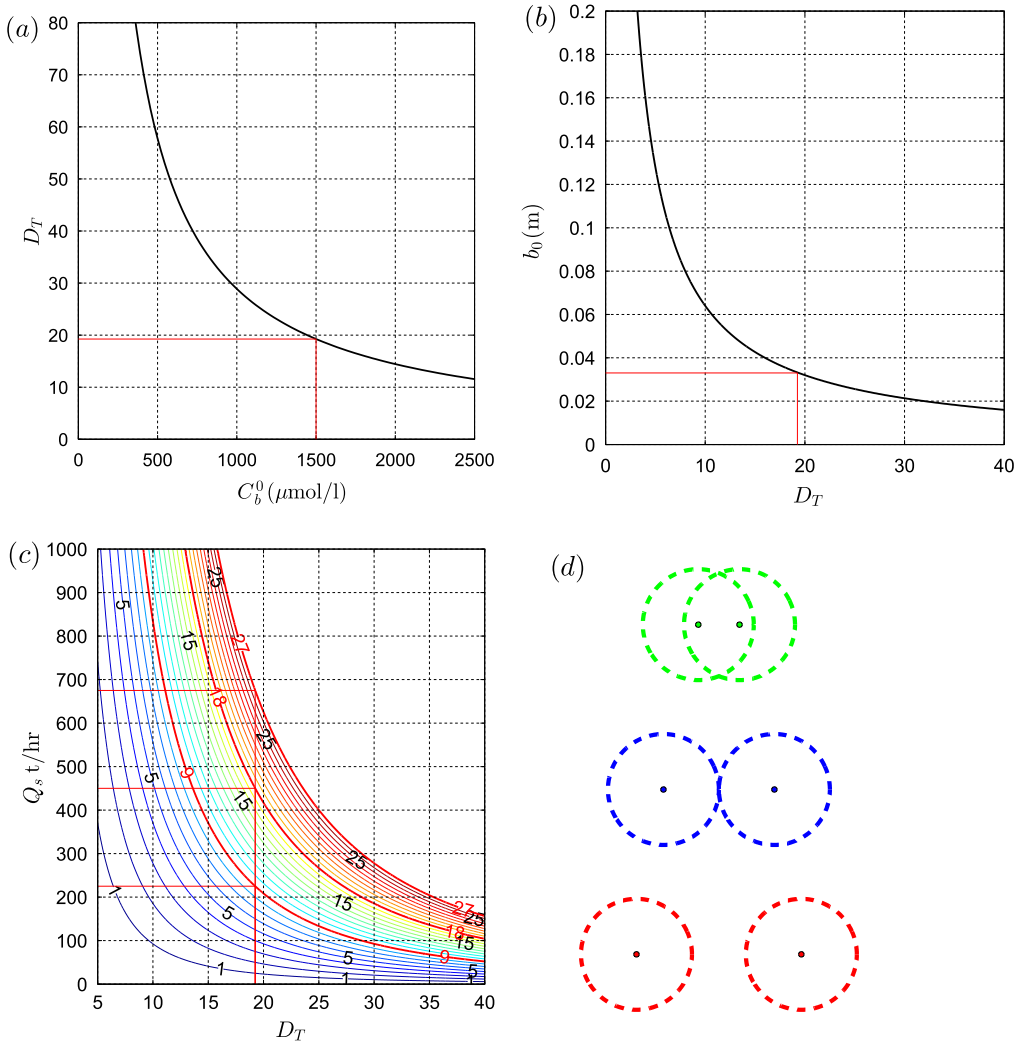

Fig. 6. In (a), the total dilution (D_T) required to give a pH of 6.5 is plotted against the alkalinity of seawater (C_b). The estimated shape of the curve is based on where the pH of 6.5 is reached in the titration experiments for River Thames and Brighton Marina. This curve should be populated with seawater samples from the relevant locations to the ship. In (b), the nozzle radius of 0.033 m required at a discharge rate of 2 m/s to reach the required dilution in the D_{jet}. In (c), the number of discharge ports required for a range of flow rates Q_s at the speed of 2 m/s and nozzle radius 0.033 m to reach the required dilution D_T for 5, 10 and 15 MW ships. In (d) the influence of separation of the discharge ports (filled circles) on the overlapping entrainment fields is illustrated (dashed lines) from the perspective of an observer looking directly along the discharge trajectory. In the case of green circles the ports (of radius 0.033 m) are separated by 0.5 m and the edges of the jet overlap reducing entrainment. The blue circles indicate optimal separation 1.35 m ($4\alpha y + 2b_0$ between the centres of the ports) and in the case of red circles the separation is 2 m resulting in excess space. (For interpretation of the references to colour in this figure legend, the reader is referred to the web version of this article.)

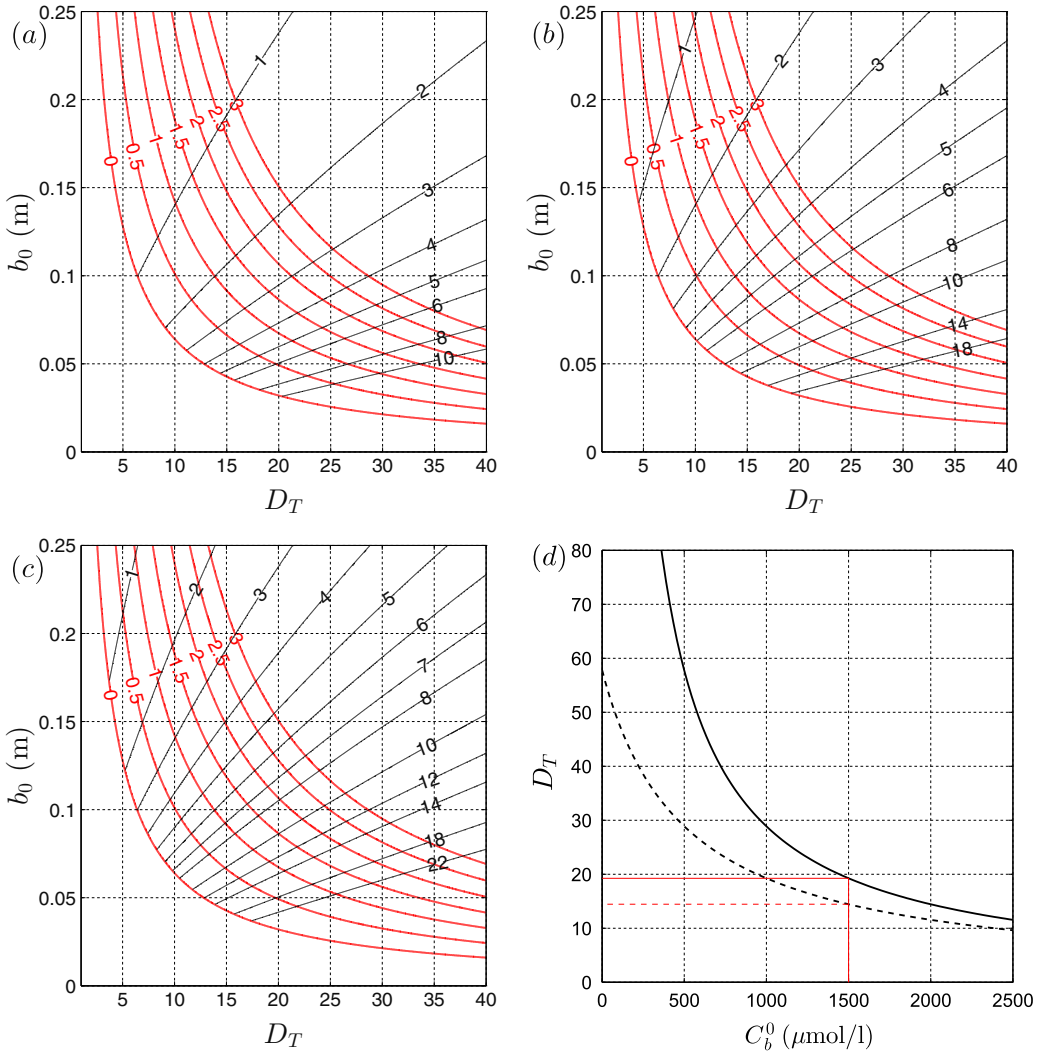

Fig. 7. In (a–c) the discharge pipe radius (b_0) is plotted against total dilution (D_T) for 5, 10 and 15 MW ships respectively. The red contour lines raise the total dilution with dilution done prior to discharge. The black contour lines highlight the number of nozzles required to achieve the necessary scrubber flow rate. The jet exit velocity at each nozzle is 2 m/s. In (d) the effect of alkali addition to the scrubber discharge is presented. The solid line corresponds to Fig. 6a and the dashed line corresponds to an addition of 500 μmol/kg of calcium carbonate to the discharge. (For interpretation of the references to colour in this figure legend, the reader is referred to the web version of this article.)

a low alkalinity of 1500 μmol l^{-1}. This alkalinity is typical for the main shipping routes in the Baltic Sea (Fig. 2b). The alkalinity determines the total dilution required which is $D_T = 19.25$ (obtained from Fig. 6a from the solid red line) and this sizes the discharge port radius which is 0.033 m from (24). We have chosen $u_0 = 2$ m/s which is a conservative estimate of the discharge speed. The number of ports is shown in Fig. 6c. The result is that for the 5, 10 and 15 MW ships 9, 18 and 27 outlet nozzles are required.

Fig. 6d showing the influence of separation of the ports (filled circles) on the overlapping entrainment fields (dashed lines) from the perspective of an observer looking directly towards the ports. Having 10 ports on the side of a ship still remains a practical solution, especially if laid out in a staggered arrangement. When the discharge port holes are close together or form of a slot, the entrainment rate is reduced because the perimeter available for entrainment is reduced. Further downstream interacting jets and plumes tend to combine into a single entity (Kaye and Linden, 2004). For example in the case of a slot of width $2b_0$, the jet radius growth and velocity decay are $b = b_0 + \alpha x$ and $u/u_0 = 1/(1 + \alpha x/b_0)^{1/2}$ respectively. Similarly to a circular jet the dilution increases with distance but at a slower rate, *i.e.* $D_{jet} = (1 + \alpha x/b_0)^{1/2} - 1$.

3.2. With prior dilution or treatment ($D_{onboard} > 0$)

For large ships and low alkaline waters, it may become impractical to add multiple discharge ports. The engineering alternative is to form a discharge tank in the hull of the ship or a sea chest with port separation as suggested in Fig. 6d. Alternatively, technologies are available that rely on multiple jets issuing from a single discharge port which could be employed. When these are not available, the remaining solution is to either add an alkaline agent at a constant rate with alkalinity C_b^{add} or to dilute onboard, both of these processes can be represented as an equivalent dilution $D_{onboard}$. In this case, the outlet port radius b_0 and number of ports N are determined from an implicit equation

Table 1
Example calculation of D and pH from experimental data.

Step	0	1	2
Beaker (ml)	114	$114 - 20 + 56 = A$	$A - 20 + 70 = B$
Acid/total (ml)	$\frac{4}{114} = C$	$\frac{114\times C - 20\times C}{A} = D$	$\frac{A\times D - 20\times D}{B} = E$
D	$C/C - 1$	$C/D - 1$	$C/E - 1$
NaOH (ml)	17.05	8.85	5.30
pH	3.45	3.73	3.95

$$D_{onboard} = \frac{1 + D_T}{1 + 2\alpha x/b_0} - 1, \quad N = \frac{Q_s(1 + D_{onboard})}{\pi b_0^2 u_0} \tag{25a, b}$$

For the results to be physically meaningful $D_{onboard} \geqslant 0$. Fig. 7a,b,c highlight the effects of onboard dilution on a 5, 10 and 15 MW ship. Fig. 7d shows the reduced need for dilution due to alkali addition of negligible volume that in essence has the effect of reducing the scrubber wash water acidity

$$C_a^0 = \frac{(C_a^s - C_b^0 - C_b^{add})Q_s}{Q_s + Q_w}. \tag{26}$$

4. Conclusions

In this paper we have examined the implications of the MEPC 59/24/Add.1 Annex 9 policy and engineering solutions to ensure compliance. The key variables to the pH recovery within the ambient seawater in which the ship operates are the turbulent discharge jet nozzle radius b_0, the alkalinity of the seawater C_b^0 and the acidity of the discharge C_a^0. The discharge flow rate Q_0 then determines the number of ports N. The practical challenge of introducing multiple ports can be met using a sea chest with circular holes. In case of either very acidic scrubber discharges or low alkalinity waters additional pH recovery can be induced by onboard dilution $D_{onboard}$ or alkali addition (see Section 3.2).

The detailed analysis has identified some specific issues related to compliance. The scrubber discharge rises due to buoyancy and it is also swept past the outlet nozzle by a flow induced by the propeller during the compliance test (the engine needs to be running and driving the screw), this leads to significant jet deflection (see Fig. 3c and d). As shown in Fig. 4d, measuring the jet dilution a distance of a jet radius from the jet centre line leads to an over estimation of dilution by a factor of 3–10 that results in a pH difference of 1–1.5 units (see Fig. 5). The likely scenario for testing scrubber discharge compliance is that a small boat is used with a person collecting samples, a potentially dangerous endeavour due to the proximity to the screw propeller, by drawing fluid from locations beneath the free surface. A number of samples need to be taken and time averaged to account for the turbulent 'flapping' of the jet and in order to get meaningful data the jet position 4 m from the ship ($y = 4$ m) needs to be estimated (see Fig. 3). The accuracy of measuring the pH at a specific depth is problematic and requires calibrated and temperature corrected probes. An alternative method to validating the discharge compliance is to measure the temperature as a series of points along the discharge jet. The temperature measurements can be used to infer the dilution at 4 m with the pH determined from titration curves.

Acknowledgement

Hendrik Ülpre would like to thank the Archimedes Foundation in Estonia for funding this work.

Appendix A

The key element to this paper are the titration experiments that need to be undertaken to determine the amount of dilution required by $D_{onboard}$ and D_{jet} to reach the pH of 6.5. A detailed overview of the example experimental procedure can be found in the following flowchart. The reason for taking out two 10 ml samples is that each one of them can be titrated against a strong base allowing for the calculation of the mean value. Litmus dye was used to determine the point of neutralisation. It is worth noting that these experiments are very sensitive to contamination and should be performed rather quickly to minimize the release of CO_2 from solution.

The important element to processing the experimental data (see Table 1) is that the number of moles of acid must be tracked as the acidified seawater is diluted. At initial conditions, step 0, the solution in the beaker consists of 100 ml of seawater, 4 ml of monoprotic acid and 10 ml of litmus solution. In step 1, two 10 ml samples are removed from the beaker and 56 ml of unacidified seawater is added. In step 2, two 10 ml samples are again removed and 70 ml of unacidified seawater is added. The pH at room temperature (25 °C) is calculated from

$$\mathrm{pH} = -\log_{10}\left(\frac{V_b}{1000} \times C_b\right), \tag{27}$$

where V_b is the volume of NaOH added in ml and C_b is the molar concentration of NaOH solution in mol/l. The example calculations are performed with the assumption that the added litmus solution had a neutral pH.

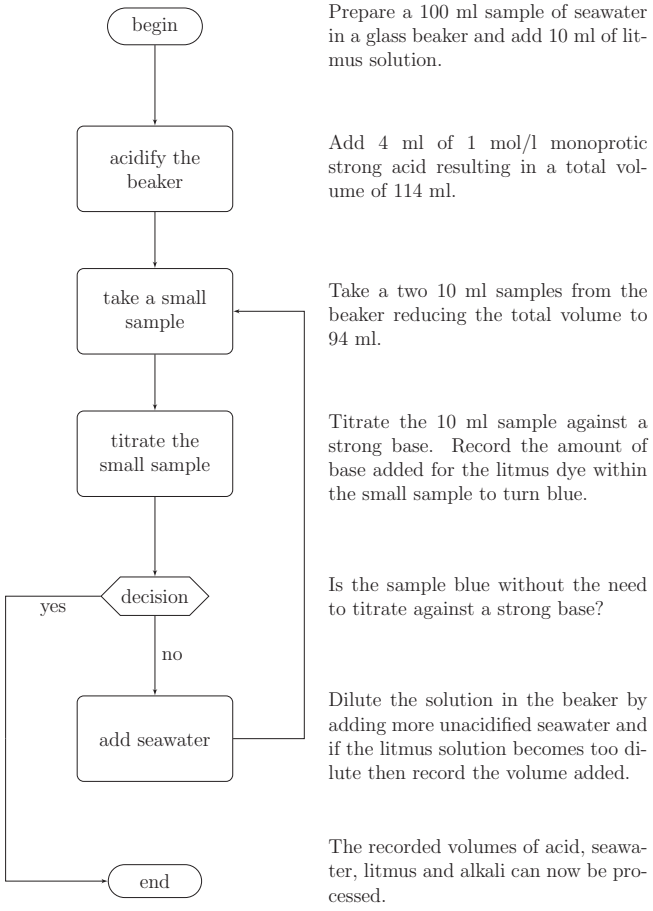

References

Abel, N., 1826. Auflösung einer mechanischen Aufgabe. J. Reine Angew. Math. 1, 153–157.
Batchelor, G., 2001. An Introduction to Fluid Dynamics. Cambridge University Press, Cambridge, UK.
Behrends, B., Liebezeit, G., Hufnagl, M., 2005. Effects on Seawater Scrubbing. BP Marine/Research Centre Terramare, UK.
Blatcher, D., Eames, I., 2013. Compliance of Royal Navy ships with nitrogen oxide emissions legislation. Mar. Pollut. Bull. 74, 10–18.
da Silva, C., Hunt, J., Eames, I., Westerweel, J., 2014. Interfacial layers between regions of different turbulence intensity. Annu. Rev. Fluid Mech. 46, 567–590.
Drever, J., 1988. The Geochemistry of Natural Waters. Prentice-Hall, Toronto, CA.

Hunt, J., Eames, I., da Silva, C., Westerweel, J., 2011. Interfaces and inhomogeneous turbulence. Philos. Trans. A Math. Phys. Eng. Sci. 369, 811–832.
ICES, 2011. Dataset on Ocean Hydrography. The International Council for the Exploration of the Sea, Copenhagen.
IMO, 2009. Second IMO GHG Study. London, UK.
Jirka, G., 2004. Integral model for turbulent buoyant jets in unbounded stratified flows. Part I: Single round jet. Environ. Fluid Mech. 4, 1–56.
Kaye, N., Linden, P., 2004. Coalescing axisymmetric turbulent plumes. J. Fluid Mech. 502, 41–63.
Key, R., Kozyr, A., Sabine, C., Lee, K., Wanninkhof, R., Bullister, J., Feely, R., Millero, F., Mordy, C., Peng, T., 2004. A global ocean carbon climatology: results from GLODAP. Global Biogeochem. Cycles 18, GB4031.
Knutzen, J., 1981. Effects of decreased pH on marine organisms. Mar. Pollut. Bull. 12, 25–29.
Krivchenko, G., 1994. Hydraulic Machines: Turbines and Pumps. Lewis Publishers, FL, USA.
McNaughton, K., Sinclair, C., 1966. Submerged jets in short cylindrical flow vessels. J. Fluid Mech. 25, 367–375.
Morton, B., 1967. Entrainment models for laminar jets, plumes, and wakes. Phys. Fluids 10, 2120–2127.
Morton, B., Taylor, G., Turner, J., 1956. Turbulent gravitational convection from maintained and instantaneous sources. Proc. Roy. Soc. London 234A, 1–23.
Raven, J., Caldeira, K., Elderfield, H., Hoegh-Guldberg, O., Liss, P., Riebesell, U., Shepherd, J., Turley, C., Watson, A., 2005. Ocean Acidification due to Increasing Atmospheric Carbon Dioxide. The Royal Society: The Science Policy Section.
Reynolds, O., 1873. The causes of the racing of the engine of screw streamers investigated theoretically and by experiment. Trans. Inst. Naval Arch. 14, 56–63.
Tanaka, M., Girard, G., Davis, R., Peuto, A., 2001. Recommended table for the density of water between 0 °C and 40 °C based on recent experimental reports. Metrologia 38, 301–309.
Turner, J., 1969. Buoyant plumes and thermals. Annu. Rev. Fluid Mech. 1, 29–44.
Ülpre, H., Eames, I., Greig, A., 2013. Turbulent acidic jets and plumes injected into an alkaline environment. J. Fluid Mech. 734, 253–274.
Woodhouse, M., Hogg, A., Phillips, J., Sparks, R., 2013. Interaction between volcanic plumes and wind during the 2010 Eyjafjallajökull eruption, Iceland. J. Geophys. Res. Solid Earth 118, 92–109.